JOURNAL OF SPACECRAFT AND ROCKETS
Vol. 47, No. 6, November–December 2010

Resolved CN Band Profile of Stardust Capsule Radiation at Peak Heating

Peter Jenniskens*
SETI Institute, Mountain View, California 94043
Michael A. Wilson†
University of California, San Francisco, San Francisco, California 94143
and
Michael Winter‡ and Christophe O. Laux‡
École Centrale Paris, 92290 Châtenay-Malabry, France

DOI: 10.2514/1.38074

During the 2006 Stardust Sample Return Capsule entry observing campaign, the highest spectral resolution data gathered onboard NASA's DC-8 Airborne Laboratory was measured with a fixed-mounted slitless cooled charge-coupled-device spectrograph, called ASTRO. Spectra were recorded around the time of peak heating ∼09 : 57 : 33 Coordinated Universal Time (UTC) on 15 January. The data covered three 0.8-second time intervals centered on 09:57:32.5, 34.4 and 36.3 s (±0.5 s) UTC, when the capsule was at an altitude of 60 and 210 km from the spectrometer. The observed spectrum was a composite of first-, second-, and third-order emissions. The first-order spectrum contained only continuum emission. Second-order emissions included the 615 nm atomic line of oxygen; third-order emissions included the CN violet 0-0 band, the isoelectric N_2^+ band, and two Ca^+ atomic lines. The Ca^+ lines had an instrumental full-width at half-maximum of 0.15 ± 0.01 nm. The CN violet band contour measured vibrational and rotational excitation temperatures of $T_v = T_r = 8,000 \pm 1,000$ K, if self-absorption is neglected.

I. Introduction

THE Stardust Sample Return Capsule (SRC) entered Earth's atmosphere at 100 km altitude with a speed of 12.82 km/s on 15 January 2006. The capsule's heat shield consisted of a phenol-impregnated carbon ablator material (PICA) [1]. The initial shape and material properties of the capsule were well known. The shield protected a cargo of dust grains collected from comet 81P/Wild 2. The physical conditions during entry were measured by remote sensing, using a range of spectrographic cameras operated behind optical windows on NASA's DC-8 Airborne Laboratory. The observing campaign set out to measure the spectral signatures of radiation escaping the shock. Coupled to studies of the recovered heat shield, this provided the first system field test of PICA.

In this paper, observations are analyzed that were made with a fixed-mounted staring slitless spectrograph, called ASTRO, designed to obtain spectra at the highest possible spectral resolution, albeit over a small wavelength range and over a brief period of time [2]. The high spectral resolution was achieved in part by recording the overlapping second- and third-order spectra, while most other spectrographic cameras recorded only the first-order spectrum. The observations are unique in that they resolved the molecular band of N_2^+ (from shock radiation) at 391.5 nm from that of isoelectric CN at 388.4 nm (a chemical product of ablated carbon atoms and air nitrogen molecules) at the time of peak heating.

Received 15 April 2008; revision received 30 April 2010; accepted for publication 3 May 2010.

*Carl Sagan Center, 515 North Whisman Road, Mountain View, CA 94043.
†Department of Pharmaceutical Chemistry; Exobiology Branch, NASA Ames Research Center, Moffett Field, CA 94035.
‡Laboratoire EM2C, Grande Voie des Vignes.

II. Instrument

ASTRO consisted of a two-stage thermo-electrically-cooled backilluminated Pixelvision charge-coupled-device (CCD) camera, equipped with a long-focal-length 300 mm f2.8 Nikon lens, and a large-format Richardson Grating Laboratory 11 × 11 cm 600 lines/mm transmission grating placed in front of the lens (Fig. 1). The instrument was mounted in one of the 62° upward-looking ports (no. 3) of the NASA DC-8 research aircraft.

The instrument was first developed for meteor spectroscopy during the 1998 Leonid Multi-Instrument Aircraft Campaign [2–5]. The camera itself has only a narrow 5 × 5° field of view, but the objective grating collects light along a 5° wideband on the sky (Fig. 1). The orientation of that band is dictated by the orientation of the dispersion direction of the grating. By choosing a long-focal-length lens and a high-dispersion grating, the instrument was capable of measuring a 138-nm-wide (in first order) part of the

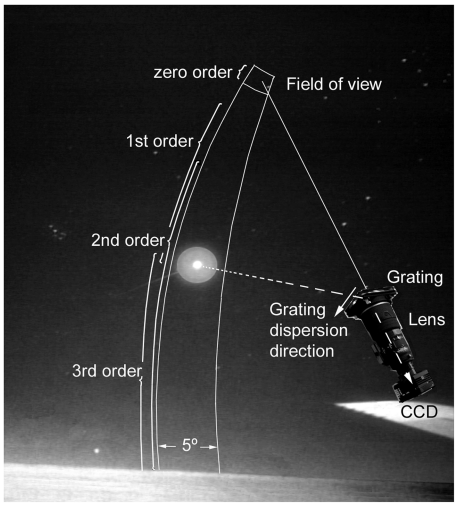

Fig. 1 Stardust entry and relative orientation of the ASTRO camera (schematic).

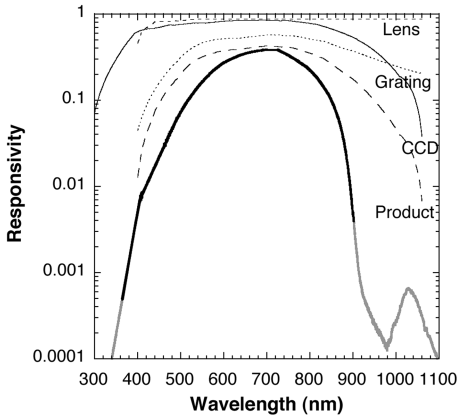

Fig. 2 Spectral response curve of the ASTRO instrument, and contributions from individual components (factory provided).

spectrum at 16-bit dynamic range from any point source that appeared in the band. The central wavelength of the recorded spectrum depended on the position of the light source away from the pointing direction of the camera. Figure 1 shows schematically what spectral order would be detected by ASTRO for different positions of the capsule on the sky.

In the case of Stardust, the path of the source was calculated in advance, so that the instrument could be aimed to capture an interesting part of the spectrum. It was set to capture the CN violet band in third order.

The CCD camera contained a large-format 1024×1024 pixel backilluminated SI003AB CCD array, with a 24×24 μm pixel size and a 24.5×24.5 mm image region, cooled to an operating temperature of 263.15 K. The readout time for such a large array was a relatively long 0.95 s, and shortened by binning in the spatial direction (see below). The exposure time was chosen to be 0.800 s, as a compromise between preventing motion blurring of background stars and minimizing the fraction of dead time from reading the CCD. Above 1000 nm, the silicon band gap effectively truncated photo production. The CCD response also fell off toward short wavelengths (Fig. 2).

The AF-S Nikkor f2.8/300D IF-ED 300 mm telephoto lens collection optics determined the size of the field of view and the short wavelength cutoff in sensitivity, which extended down to about 360 nm (Fig. 2). The lens was focused on the background stars.

The grating dispersion was chosen to cover the full second-order spectrum, and part of the third order. *Second order* here refers to the integer wavelength difference of 2 for diffractions from two neighboring grating grooves. Based on this, an 11×11 cm plane transmission grating no. 35-54-20-660 was used with aluminum coating on 12 mm BK7 substrate. Grating and detector were positioned such that the dispersion occurred along the rows of the CCD. This configuration provided a full second-order spectrum out to about 925 nm. A blaze wavelength of 698 nm (34°) was measured. The factory grating specifications suggested a good sensitivity out to about 1100 nm, but the measured instrument response fell off rapidly above 850 nm (Fig. 2) [2]. This discrepancy between the factory-provided product response (dashed line) and the measured instrument response may be due to the different illumination conditions of the grating in our application. No order separation filter was used. As a result, the near-UV part of the third-order spectrum was also captured, which overlapped the second-order spectrum above 540 nm (3×360 nm $= 2 \times 540$ nm).

The instrumental response in the second order has the same spectral shape as in first order (Fig. 2), at least over the range of 570–710 nm. The light is distributed over twice the number of pixels and only 2.4% of all light goes in second order to that side. By using a 10-nm-wide narrowband filter centered at 390 nm, we measured that 32.9% of all light is put in the first order to the dispersion side measured during the observations, while 2.4% goes in second order to that side, and 4.9% in third order [2]. The zero order remains 31.6% of all light [2]. For example, the third-order spectral response (ADU/pixel per $W/m^2/nm$) at a given wavelength is that shown in Fig. 2, multiplied by $0.049/0.329$ and divided by 3. Here, ADU stands for analog-to-digital unit and signifies the pixel intensity value.

The instrument was fixed-mounted at an upward-looking angle of 53° (Fig. 1). The port contained a flat borosilicate (Pyrex) window with MgF_2 antireflection coating (no. S/N156) [6]. The transmission properties of the window from 400–2500 nm were measured in the laboratory shortly after the mission, and found to vary from 0.909 at 530 nm to 0.924 at 620 nm. The shorter-wavelength transmission (less than 400 nm) was taken from older measurements on file. The transmission decreased from about 0.860 at 415 nm to 0.80 at 355 nm.

At the time of the reentry, an operator instructed the camera to record data whenever a spectrum was detected. The CCD frames were written to a laptop computer, with a time marker that specified the time of writing. The computer clock was set by hand, using a Global-Positioning-System-controlled IRIG-B timecode signal as guidance. The uncertainty is about ± 0.5 seconds. During each exposure, the SRC moved through the field of view, creating a spectral band (Fig. 3). The CCD frames were binned perpendicular to the dispersion direction (1×4), in the direction of motion of the capsule to speed up the CCD readout. This left about 37 individual spectra (rows) per exposure.

III. Results

Three spectra (Fig. 3) were written to disk at 09:57:32.9, 34.8 s, and 36.7 s $\pm$ 0.5 s Coordinated Universal Time (UTC). Based on these recording time stamps, the central time of each exposure was at about 09:57:32.5, 09:57:34.4, and 09:57:36.3 UTC, respectively, around the time of peak heating ($\sim$09 : 57 : 33 UTC).

At 09:57:34.4 UTC, the SRC was at an altitude of 60.58 km, moving relative to the atmosphere with a speed of 10.92 km/s. From the perspective of the aircraft, the capsule was at a distance of 211.2 km, and seen at an elevation of 12.28° above the horizon. The capsule was oriented 19.84° out of the line of sight, projecting 0.489 m^2 of surface area. The viewing angle difference between the pointing direction of the CCD camera and the elevation of the capsule (Fig. 1) was 45.6° along the dispersion direction (which was slightly tilted from the normal).

Additional images were taken in the seconds following the Stardust SRC passage. These background images were subtracted from the capsule's images, residual star images removed, and the values for pixel intensity were retrieved. The individual rows were then aligned, matching up the strongest lines in the spectrum, and the result was corrected for vignetting. The first spectrum (when the SRC entered the field of view) consisted of 29 pixel rows, the second spectrum had 37 (29 rows with no overlapping star spectrum), and the third spectrum was 39 pixels wide, for a total of 97 usable spectra (recorded at a rate of about 48 spectra per second).

The spectra were extracted and pixel intensity (in ADU) was averaged along pixel rows representing the same wavelength. No differences were detected among the spectra in an individual exposure, except for a gradually stronger continuum emission. The stronger continuum emission is shown in Fig. 3 as a gradual increase in brightness in time. Because of that, all usable spectra over the whole time interval (09:57:32.1–09:57:36.7 UTC) were scaled to match the 09:57:34.4 spectrum's continuum intensity and averaged. The result in Fig. 4 shows the measured average pixel intensity for each row of pixels that correspond to a given wavelength. With the capsule moving at 38 rows per 0.8 s exposure, the average intensity corresponds to an 0.021 s exposure per pixel.

This spectrum is a composition of the response in first, second, and third order. Spectral features were identified based on the known angle between viewing direction and SRC, and from the characteristic pattern of the CN band and Ca^+ lines, which were also detected by the slitless spectrograph called ECHELLE (echelle-based spectrograph for the crisp and high efficient detection of low light emission) [7] and the slit-based spectrometer called SLIT [8]. The recorded spectrum contains continuum emission in first order,

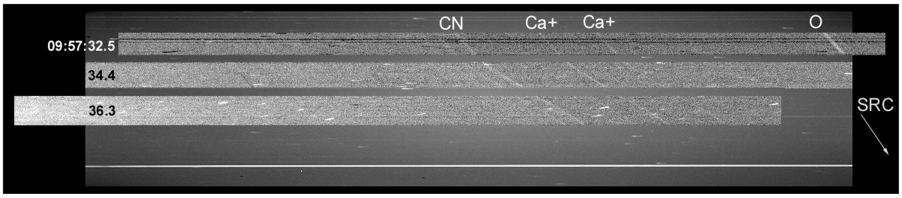

Fig. 3 Three ASTRO spectra of STARDUST SRC radiation at 09:57:32.5, 09:57:34.4, and 09:57:36.3 UTC. Wavelength increases toward the right. The background image is the full frame of the second exposure, without background subtraction and contrast enhancement.

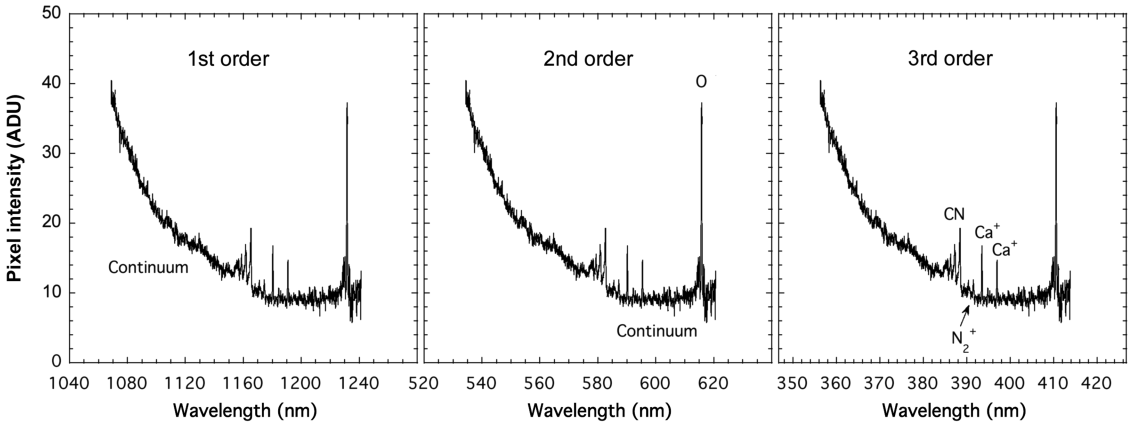

Fig. 4 Identification of emission lines and bands in the various spectral orders.

the 615 nm oxygen line (and continuum) in second order, and the CN violet $\Delta\nu = 0$ band, isoelectric N_2^+, and two Ca^+ lines in third order (Fig. 4).

IV. Calibration

The wavelength scale was calibrated from the recorded spectra using the known position of identified emission lines. Vacuum wavelengths were obtained from the Kurucz tables [9]. The scale is linear, with a dispersion of 0.0451 ± 0.0002 nm/pixel in third order, and 0.0677 ± 0.0003 nm/pixel in second order.

The relative instrumental response was calibrated using an Ocean Optics HG-1 Mercury Argon wavelength calibration source and an Ocean Optics LS-1-CAL tungsten calibration lamp (LSC207). These two small lamps each have a 3 mm opening aperture (a SMA 905 connector for optical fiber), small enough to act as near point sources when placed at some distance from the camera. The lamps were positioned on top of each other. In this way, the line source provided a wavelength scale for the continuum emission. The ASTRO instrument was pointed away from the direction of the lamp, in small steps, to scan the response over the whole spectrum and all orders. After correcting for vignetting and the geometric dilution factor, the response curve (Fig. 2) was constructed by means of the Ocean Optics provided lamp irradiance calibration values, correcting for the wavelength-dependent throughput of the fiber used to measure these calibration curves [7].

The absolute scale of the calibration was calculated by measuring the zero-order response of the instrument to background stars (through the aircraft window, at the time of the SRC observation). At the time of the observation, the camera was pointed to right ascension of 6 h, 55 m, 39 s and declination of $+46^\circ\ 11'\ 47''$, toward a region on the border of the constellations Lynx and Auriga (Fig. 5).

Astrophysical data of the apparent brightness of stars in the field were collected from the astronomical SYMBAD database. The data pertain to no-atmosphere conditions for five wavelength bands centered at 444, 548, 650, 750, and 850 nm. From the reported stellar spectral type and photometric magnitudes, the flux in 100 nm intervals from 400 to 900 nm was calculated. Each band was corrected for relative instrumental response (Fig. 2), for window transmission, and for atmospheric extinction (the star viewing elevation at that time being 51°). Then the sum pixel intensity of all stellar images (in ADU units on the same 8-bit scale as for the reduced spectra) was plotted against the integrated flux density of each star (Fig. 6).

A least-squares fit gives a response of $1.52 \pm 0.07 \times 10^{15}$ ADU per W/m^2, with the ADU pixel intensity (16-bit) summed over all pixels of the zero-order star image during an 0.8 s exposure (Fig. 6). The zero-order star images contain the integrated light over the full wavelength range over which the camera is responsive. The integral of the responsivity curve of Fig. 2 equals 90.2 nm x responsivity units. Such stationary sources also integrate light during the full exposure, instead of just during the time that the SRC moves over one pixel. Hence, the wavelength-dependent instrumental response is derived by multiplying Fig. 2 with the scale

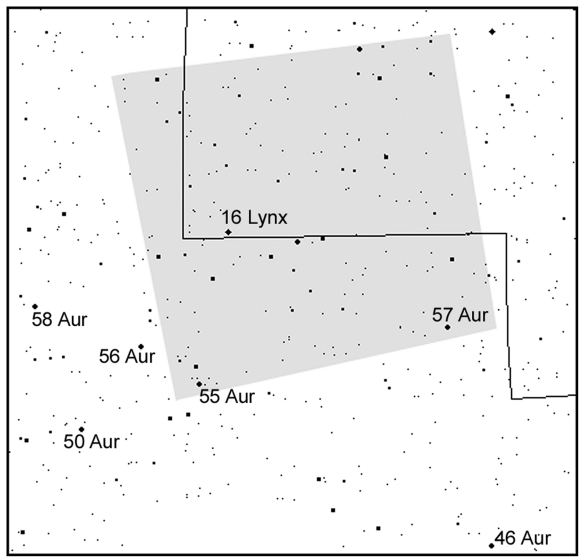

Fig. 5 Identification of background stars in the camera field (gray). Stars with Flamsteed numbers in the constellations Lynx and Auriga are labeled.

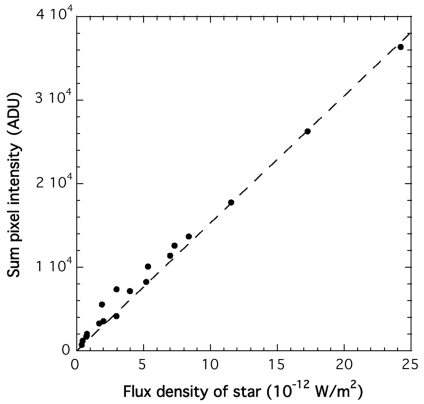

Fig. 6 Calibration curve relating apparent stellar flux density to the sum of pixel intensity values in the unscaled 16-bit images exposed during 0.8 s (see text).

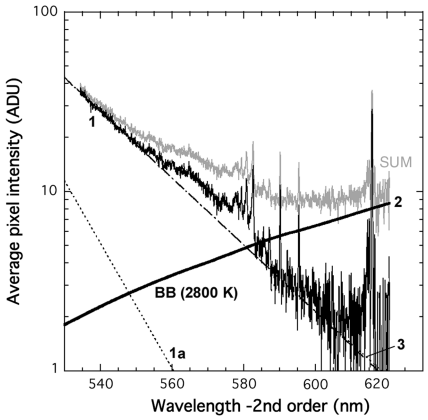

Fig. 7 Decomposition of the contribution from first (dashed-dotted line) and second (solid line, wavelength scale) spectral orders, both adding to the third order to create the observed (Sum) spectrum. The dotted line is explained in the text.

factor $1.52 \pm 0.07 \times 10^{15}$ ADU per W/m^2, dividing by the integral of Fig. 2, and correcting for the difference in pixel exposure time.

V. Decomposition

The observed pixel intensity is a sum of contributions from the three orders. With $E^{\circ}(\lambda)$ the flux density just outside of the aircraft window (corrected for telluric extinction), ϕ^i the instrument responsivity shown in Fig. 2, the spreading of light over number of pixels in each order $\phi^o = m$ for order m, $\phi^f =$ fraction of light in order m divided by fraction of light in zero order, ϕ^e the telluric extinction, ϕ^w the window extinction, ϕ^g the geometric dilution, and Δt the exposure time for a single pixel (0.021 s), the average pixel intensity (in ADU) is given by

$$I_{\text{pix}} = \Delta t(\text{pix})/0.8 * \Sigma_{m=1,3} E^o(\lambda) * \phi^i_m(\lambda) * 1.52 \times 10^{15}/90.2/\phi^o(m) * \phi^f(m) * \phi^e_m(\lambda) * \phi^w_m(\lambda) * \phi^g \quad (1)$$

Because the SRC is detected away from the viewing direction, a $\phi^g = \cos(45.5^{\circ})$ geometric dilution factor needs to be taken into account, where 45.5° is the average tilt of the grating from the perspective of the capsule at the time of the observation.

The wavelength-dependent atmospheric extinction $\phi^e_m(\lambda)$ between SRC and observer (factor $\phi^e_2 \sim 0.78$ in second order and $\phi^e_3 = 0.55$–0.73 in third order) was calculated with ModTran, for the known altitude of aircraft and capsule. Results were calculated for an altitude of 60 km and elevations of 10 and 15°, and interpolated to the observed elevation of 12.5°. The aircraft altitude did not change during the observation. The total ozone column density over Nevada for 15 January 2006, was published by the World Ozone and Ultraviolet Radiation Data Center at about 320 UD (Dobson units) [8]. The aerosol concentration was assumed to be normal. Aerosols add to the extinction, but with no noticeable spectral variation.

The approach taken to decompose these contributions is not unique and relies heavily on the known shape and flux levels measured in other observations at lower spectral resolution obtained with the digital imager (DIM), near-infrared spectrograph (NIRSPEC), intensified imaging spectrograph (INT1), SLIT, and ECHELLE instruments [7,8].

The first-order emission dominated the rapid exponential decrease of intensity toward longer wavelengths (Fig. 7). In the first quarter of the spectrum is no contribution from third order, because the instrumental response curve falls off rapidly below 368 nm, where the Nikon lens is opaque (Fig. 2). The assumption was made that all emission short of 1100 nm (after subtracting the second-order component) was due to first-order continuum, with a small contribution from a second-order continuum. The exact shape of this contribution depended on the instrument's spectral response between 1070 and 1240 nm (Fig. 2). Unfortunately, this response was difficult to measure, because of overlapping second-order emission, and because it is weak. The measured emission between 1070 and 1100 nm (Fig. 4) implied an exponential falloff with a slope ≥ 0.0185 nm^{-1}, or about -0.022 ± 0.002 nm^{-1} after taking a second-order continuum contribution into account (Fig. 7, labeled 1, dashed-dotted line). The measured response (Fig. 2) in this range was exponential in slope, but slightly steeper at -0.030 ± 0.003 nm^{-1} (in the range 1070–1100 nm), perhaps steepening to -0.041 nm^{-1} between 1100 and 1150 nm (Fig. 7, labeled 1a, dashed line).

The second-order continuum contribution dominated the emission in the final quarter of the spectral range, between second-order wavelengths 580 and 620 nm (Fig. 4). The capsule's flux density was nearly wavelength independent (gray) in this range. Except for the 615 nm lines of oxygen, centered on 615.79 nm (in vacuum), no strong emission lines were detected by ECHELLE in the 530–620 nm range a few seconds earlier in flight at 09:57:26 UTC [7]. The sodium lines at 589.158 and 589.756 nm, which would have been well resolved, were not detected, neither were the weak nitrogen lines at 575.4 and 577–8 nm.

Based on the known distance and effective surface area of the capsule, and assuming an emissivity of 0.88, the expected blackbody emission in the 580–620 nm range was calculated. A temperature of 2800 K resulted in emission strong enough, when subtracted from Fig. 4, to cause a first-order continuum at longer wavelengths to match the exponential decrease at short wavelengths (Fig. 7). Temperatures in the range 2600–3300 K would all produce a flat continuum needed to produce such an exponential falloff.

That same continuum is almost negligible in third order (Fig. 7, labeled 3, dotted line). Instead, all third-order emissions are from the CN molecular band profile and from two atomic emission lines of Ca^+. We notice that the recorded signal below 368 nm is exponential in shape, with a slope of -0.0395 per first-order wavelength in nm (Fig. 7). This exponential slope is subtracted from the spectrum and the result, now free of second- and first-order continuum emission, is multiplied by the third-order response (Fig. 8). After subtracting the first- and second-order continuum contributions, what remains is third-order emissions (Fig. 8).

To check the validity of the procedure, the result was compared to the flux density measured by the SLIT instrument in the same time frame (shown by a thin line in Fig. 8). Note that SLIT was a bench-mounted slit spectrograph that was fed by an optical fiber aimed at the capsule with a small telescope. Because of pointing inaccuracies, the signal sometimes drops off. The intensity of the SLIT spectrum was matched to the upper contour of emissions from other nearby spectra taken in this time interval. Note how the spectral resolution of ASTRO in third order is about a factor of 4 better than that of SLIT (0.15 nm versus 0.60 nm resolution).

A broad feature is present in the ASTRO spectrum that is not seen in SLIT, and therefore must be a feature of either the second- or first-order part of the spectrum. Figure 8 shows this feature assuming that it is part of the second-order emission. It is centered on 564 nm and about Gaussian in shape, with a width sigma = 6.0 nm. If this was a

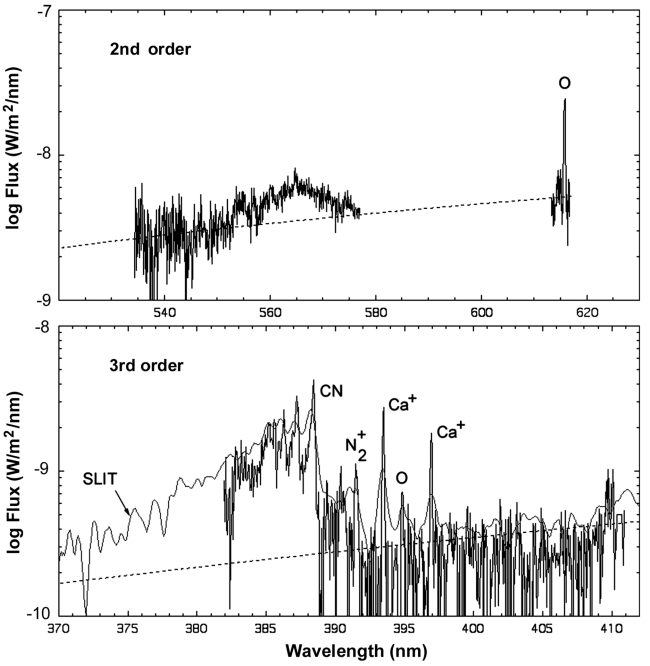

Fig. 8 Apparent flux from the Sample Return Capsule at the aircraft at the time of peak heating in third order (below) and in second order (above).

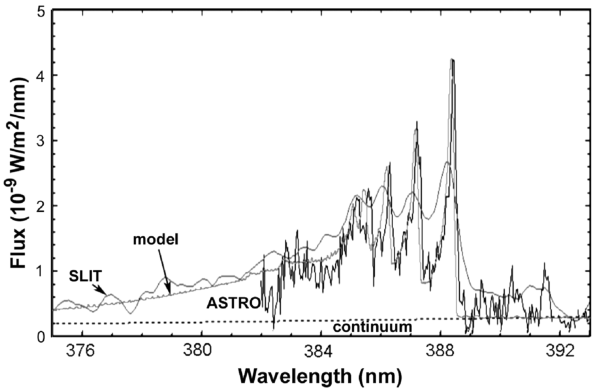

Fig. 9 Model SPECAIR fit (gray line, slightly displaced) to ASTRO and SLIT data, for $T_v = T_r = 8,000$ K.

feature of the first-order spectrum, it would be centered at 1128 nm and be twice as wide. It is possible that the broad feature is due to an irregularity in the first-order response curve. In the same way, the narrow line at 563 nm (Fig. 8) could be the 1028 nm line of oxygen in first order (Fig. 4).

VI. Interpretation

The results are available now for further interpretation in combination with other Stardust SRC entry data sets and numerical flow and radiation modeling.

As an example, the 0-0 band of CN measured in third order was fitted using SPECAIR [10], with a Gaussian slit function with full-width at half-maximum of 0.15 ± 0.01 nm (from the observed line width of the Ca^+ lines in third order). The result is shown in Fig. 9, with the model spectrum being lightly displaced for clarity. The best fit was obtained for a vibrational temperature being the same as the rotational temperature $Tv = Tr = 8,000\ \text{K} \pm 1,000\ \text{K}$. Lower temperatures resulted in a more rapid decline of the strength of band heads toward shorter wavelengths. Band heads of isoelectric N_2^+ suggest a similar high temperature.

VII. Conclusions

The combined first-, second-, and third-order emissions detected by the ASTRO instrument were successfully retrieved and fully calibrated against the background stars. The data provide high-spectral-resolution measurements at the time of peak heating in three wavelength intervals: from about 382 to 409 nm, from 535 to 577 nm, and in a small interval around 615 nm. The derived rotational and vibrational temperatures of the CN molecules are of order $Tv = Tr = 8000 \pm 1000$ K. Oxygen line emission is detected at 615 nm, and perhaps also at 394 nm, the intensity of which may be used to evaluate the level of radiative heating [11]. A broad emission feature centered on 563 nm (if second order) remains unidentified. It might be due to an irregularity in the first-order response of the camera.

The observations of the Stardust Sample Return Capsule entry are expected to remain a unique system field test for a long time to come. The measured rotational and vibrational excitation temperatures might inform future studies into the conditions of carbon atom ablation, their reaction with air molecules, and the penetration depth of the carbon atoms into the shock layer. The observational data and the calibration files have been archived for this purpose. The present paper serves to document the files released on 31 March 2008.

Acknowledgments

NASA's DC-8 Airborne Laboratory was deployed by the University of North Dakota and National Suborbital Education and Research Center, under contract with NASA Wallops Flight Center. This work was funded and managed by the Orion Thermal Protection System Advanced Development Project and the NASA Engineering and Safety Center. Dave E. Jordan of NASA Ames Research Center acted as the NASA Program Manager for the mission and designed methods for instrument installation.

References

[1] Jenniskens, P., Kontinos, D., Jordan, D., Wright, M., Olejniczak, J., Raiche, G., et al. , "Preparing for the Meteoric Return of Stardust," *Dust in Planetary Systems*, SP 643, edited by A. Grapps, and E. Gruen, ESA, Paris, 2006.

[2] Jenniskens, P., "Quantitative Meteor Spectroscopy: Elemental Abundances," *Advances in Space Research*, Vol. 39, 2007, pp. 491–512. doi:10.1016/j.asr.2007.03.040

[3] Jenniskens, P., and Butow, S. J., "The 1998 Leonid Multi-Instrument Aircraft Campaign—An Early Review," *Meteoritics And Planetary Science*, Vol. 34, 1999, pp. 933–943. doi:10.1111/j.1945-5100.1999.tb01411.x

[4] Jenniskens, P., and Russell, R. W., "The 2001 Leonid Multi-Instrument Aircraft Campaign—An Early Review," *Institute of Space and Astronautical Science Report S.P.*, Vol. 16, 2003, pp. 3–15.

[5] Jenniskens, P., Schaller, E. L., Laux, C. O., Schmidt, G., and Rairden, R. L., "Meteors Do Not Break Exogenous Organic Molecules into High Yields of Diatomics," *Astrobiology*, Vol. 4, 2004, pp. 67–79. doi:10.1089/153110704773600249

[6] "DC-8 Experimenters Hand Book," NASA Dryden Flight Research Center, 2003.

[7] Jenniskens, P., "Observations of the Stardust Sample Return Capsule Entry with a Slitless Echelle Spectrograph," *Journal of Spacecraft and Rockets*, Vol. 47, No. 5, 2010, pp. 718–735. doi:10.2514/1.37518

[8] Winter, M., and Herdrich, G., "Spectroscopic Observation of the Stardust Re-Entry in the Near UV," 39th AIAA Thermophysics Conference, AIAA Paper 2007-4050, Miami, FL 25–28 June 2007.

[9] Smith, P., "Kurucz Atomic Linelist," Harvard-Smithsonian Center for Astrophysics, Cambridge, MA, 2008, http://www.cfa.harvard.edu/amp/ampdata/kurucz23/sekur.html [retrieved 30 April 2010].

[10] Laux, C. O., "Optical Diagnostics and Radiative Emission of Air Plasmas," Ph.D. Thesis, Stanford Univ., Stanford, CA, Aug. 1993, p. 223.

[11] Trumble, K. A., Cozmuta, I., Sepka, S., and Jenniskens, P., "Post-Flight Aerothermal Analysis of the Stardust Sample Return Capsule," 46th Aerospace Sciences and Exhibit, AIAA Paper 2008-1201, Reno NV, Jan. 2008.

D. Kontinos
Guest Editor